# Comparison of different computed radiography systems: Physical characterization and contrast detail analysis

Stefano Rivetti
*Servizio Fisica Sanitaria, "Azienda USL di Modena", 41100 Modena, Italy*

Nico Lanconelli[a)]
*Department of Physics, Alma Mater Studiorum, University of Bologna, Viale Berti Pichat 6/2, 40127 Bologna, Italy*

Marco Bertolini and Andrea Nitrosi
*Arcispedale Santa Maria Nuova, 42123 Reggio Emilia, Italy*

Aldo Burani
*"Azienda USL di Modena", Ospedale di Sassuolo, 41049 Sassuolo, Italy*

Domenico Acchiappati
*Servizio Fisica Sanitaria, "Azienda USL di Modena", 41100 Modena, Italy*

(Received 16 June 2009; revised 9 November 2009; accepted for publication 29 November 2009; published 6 January 2010)

**Purpose:** In this study, five different units based on three different technologies—traditional computed radiography (CR) units with granular phosphor and single-side reading, granular phosphor and dual-side reading, and columnar phosphor and line-scanning reading—are compared in terms of physical characterization and contrast detail analysis.
**Methods:** The physical characterization of the five systems was obtained with the standard beam condition RQA5. Three of the units have been developed by FUJIFILM (FCR ST-VI, FCR ST-BD, and FCR Velocity U), one by Kodak (Direct View CR 975), and one by Agfa (DX-S). The quantitative comparison is based on the calculation of the modulation transfer function (MTF), noise power spectrum (NPS), and detective quantum efficiency (DQE). Noise investigation was also achieved by using a relative standard deviation analysis. Psychophysical characterization is assessed by performing a contrast detail analysis with an automatic reading of CDRAD images.
**Results:** The most advanced units based on columnar phosphors provide MTF values in line or better than those from conventional CR systems. The greater thickness of the columnar phosphor improves the efficiency, allowing for enhanced noise properties. In fact, NPS values for standard CR systems are remarkably higher for all the investigated exposures and especially for frequencies up to 3.5 lp/mm. As a consequence, DQE values for the three units based on columnar phosphors and line-scanning reading, or granular phosphor and dual-side reading, are neatly better than those from conventional CR systems. Actually, DQE values of about 40% are easily achievable for all the investigated exposures.
**Conclusions:** This study suggests that systems based on the dual-side reading or line-scanning reading with columnar phosphors provide a remarkable improvement when compared to conventional CR units and yield results in line with those obtained from most digital detectors for radiography.  [DOI: 10.1118/1.3284539]

Key words: computed radiography, columnar phosphor, line-scanning, dual-side reading, DQE

## I. INTRODUCTION

Digital radiography systems are replacing films over a broad range of examinations. Historically, the first step toward digital imaging is due to the introduction in the radiology scenario, a few decades ago, of the storage phosphor plates. To our days, computed radiography (CR) systems are a widespread mean to acquire radiographic examinations.[1–4] A major advantage of CR systems is that they are a cost effective way for getting digital images since they allow the reutilization of the existing x-ray equipment. CR cassettes utilize storage phosphors where electrons trapped during the exposure are subsequently extracted from traps through a laser scanner. The effect exploited by CR systems is known as "laser-stimulated luminescence." After the reading step, the cassette is erased with a process which extracts all the remaining trapped electrons. It is then possible to proceed with a new exposure. Conventional CR systems are based on screens composed of granular phosphors and reading scanners that employ a single-side spot reading (i.e., the laser impinges the phosphor only at one point on one side).

Since its introduction, CR has been continuously improved and two major advances have been introduced in the scenario during the past few years. In the first place, new reading scanners have been developed either reading the phosphors from both sides or through the line-scan technology.[5–7] In the "dual-side" reading, the support plate is

TABLE I. The investigated CR imaging systems and their principal characteristics.

| | | | | | |
|---|---|---|---|---|---|
| Manufacturer | FUJIFILM Medical Systems | FUJIFILM Medical Systems | Eastman Kodak | FUJIFILM Medical Systems | Agfa HealthCare |
| Model | FCR Profect CS | FCR Profect CS | CR975 | FCR Velocity | DX-S |
| IP type | ST-VI | ST-BD | GP | FP | HD |
| Phosphor type | Granular: BaFBr($Eu^{2+}$) | Granular: BaFBr($Eu^{2+}$) | Granular: BaFBr($Eu^{2+}$) | Columnar: CsBr($Eu^{2+}$) | Columnar: CsBr($Eu^{2+}$) |
| Phosphor thickness ($\mu$m) | 230 | 320 | 300 | 650 | 450 |
| Reader type | Single-side reading | Dual-side reading | Single-side reading | Line scanning | Line scanning |
| Imaging area ($cm^2$) | $24\times30$ | $24\times30$ | $35\times43$ | $43\times43$ | $35\times43$ |
| Array size | $2364\times2964$ | $2364\times2964$ | $2048\times2500$ | $4280\times4280$ | $3408\times4200$ |
| Pixel pitch ($\mu$m) | 100 | 100 | 168 | 100 | 100 |
| Image depth (bits) | 10 | 10 | 12 | 10 | 14 |

made of a transparent material which allows reading the light both from the "front" and the "rear" sides of the cassette. In this case, two optical subsystems are included into the reading scanner. In the "line-scan" technique, the phosphor plate is scanned one line at a time rather than one point at a time. This is done by illuminating the cassette with a linear array of lasers. These two reading modalities allows for an enhanced detection efficiency and a fast readout of the entire image. In the second place, columnar phosphors have been introduced for CR cassettes, usually based on CsBr crystals.[8–10] That allows light to be channeled out of the screen with little lateral spread, making it possible to use thicker screens, thus improving absorption efficiency without much loss in the spatial resolution.

Some of the systems investigated in this work were already analyzed by other studies in the past years.[5,11,12] However, no direct objective comparison has been made on the basis of the same exposure conditions. The aim of this paper is to achieve a direct comparison among various CR systems based on three different technologies and marketed by three of the major manufacturers on the basis of the same exposure conditions. This study presents a summary of the performance of the currently available CR systems by comparing the basic objective image performance characteristics of resolution, noise, and detective quantum efficiency (DQE). In addition, we are also performing the comparison in terms of contrast detail (CD) analysis, thus providing a more complete evaluation of the various systems. Here, we analyze five different CR systems based on photostimulable storage phosphor. These systems are based on different technologies, such as granular or columnar phosphors, single-side, dual-side, or line-scanning techniques. Two systems are based on the conventional granular phosphor with a single-side laser scanner technology. Another one utilizes the same granular phosphor and a dual-side reading scanner. The last two systems are based on columnar phosphors and line-scanning technique—the latest technology available. We have assessed the physical characterization in terms of spatial resolution and noise analysis. Specifically, the modulation transfer function (MTF), noise power spectra (NPS), relative standard deviation (RSD), and DQE have been estimated for all the systems using the same acquisition setup. A CD analysis has also been performed using the CDRAD phantom (Artinis, Medical Systems B.V., Zetten, The Netherlands). The CDRAD phantom can help in the assessment of the imaging characteristics of digital radiographic systems and is used to evaluate their contrast detail response. An automatic reading of the phantom was obtained with a software developed by our group.[13] The overall goal is to provide a characterization for some of the most common photostimulable phosphor based systems available on the market and determine the variations in physical parameters due to the different technologies employed.

## II. MATERIALS AND METHODS

The five systems analyzed in this paper are three FUJIFILM units, namely, one FCR Profect CS Reader with ST-VI plate (FCR ST-VI), one FCR Profect CS Reader with ST-BD plate (FCR ST-BD), one FCR Velocity U Reader with FP plate (FCR Velocity), one Kodak unit, Direct View CR 975 Reader with GP plate (CR 975), and finally, one Agfa unit, DX-S Reader with HD plate (DX-S). All the units are currently used in radiology departments and their main characteristics are summarized in Table I. The FCR ST-VI and CR 975 units are based on the well-known CR technology consisting of granular phosphors and single-side flying spot readers. The FCR ST-BD unit applies a dual-side reading system to the same granular phosphor cassettes used in the previous two systems. The last two systems (FCR Velocity and DX-S) are based on columnar phosphors and line-scanning readers—the latest technology available on the market. The line scanning technology employs a CCD detector for reading the light. All measurements were made using a common radiographic technique. Specifically, a fixed tube voltage equal to 70 kVp with 21 mm additional aluminum filtration (IEC Standard 61267: Standard beam condition RQA5) have been used.[14] In all image acquisitions, the exposure to the detector was measured using a calibrated ionization chamber (UNFORS Xi, Unfors Instruments, Billdal, Sweden). The source-to-image distance was nearly 180 cm for all the systems.

### II.A. Physical characterization

The response curve of all the systems was determined by exposing the detector to a wide range of uniform x-ray exposures. At each exposure, we estimated the average pixel values from a ROI located at the center of the detector. The

five clinical CR systems' physical characteristics were then analyzed in terms of MTF, NPS, and DQE. Presampling MTF was measured, adopting the well-known edge technique.[15,16] An oversampled line spread function was derived by slightly rotating (about 2°–4°) a tungsten edge test device (TX 5, IBA Dosimetry, Schwarzenbruck, Germany) with respect to the direction along which the MTF was being measured. The MTFs were measured in both the horizontal and vertical directions. For DQE calculation, the average of the MTF along the two directions was considered. NPS was computed by using flat field images at three different exposure levels (around 2.5, 5, and 10 $\mu$Gy). For each exposure level, four images were acquired. A fixed ROI was extracted from each image and subdivided into $256\times256$ regions. The 2D normalized noise power spectrum (NNPS) was then derived by averaging square modulus of the Fourier transform of each sub-ROI. Finally, the result was normalized for the square mean signal value of the ROI. The 1D NNPS was then extracted from the 2D NNPS on a radial direction at 45°, excluding the values along the axes. Noise was also studied through an RSD analysis.[17] We estimated the RSD on the same ROIs used for NNPS calculation. We then fitted the experimental RSD data computed over all the ROIs with the following function:

$$\mathrm{RSD}^2=\left(\frac{\sigma_{\mathrm{TOT}}}{x}\right)^2=\frac{\alpha}{x}+\beta+\frac{\gamma}{x^2}, \tag{1}$$

where $x$ is the x-ray exposure, while $\alpha$, $\beta$, and $\gamma$ are the contributions of the quantum-statistical (Poisson) noise source of a dose related (multiplicative) noise source and of a dose independent (additive) noise source, respectively.[17] The additive factor can be interpreted as the noise connected to electronics (e.g., dark current), whereas the multiplicative component could be related to a structured noise arising from variations in sensitivity across the detector.

The photon number per unit area $q$ was derived from tabulated values for the standard RQA5 beam. We then calculated DQE combining 1D NNPS curves with the fluence measures and the corresponding MTFs in order to get the final DQE curves,

$$\mathrm{DQE}(f)=\frac{\mathrm{MTF}^2(f)}{\mathrm{NNPS}(f,q)\cdot q}, \tag{2}$$

where $f$ is the spatial frequency and $q$ is the photon number per unit area.

### II.B. Contrast detail analysis

CD analysis was done using the CDRAD 2.0 phantom (Artinis, Medical Systems B.V., Zetten, The Netherlands). Such a phantom was developed with the purpose of estimating the perception of details on a range of sizes and contrasts and is composed of 225 squared cells organized as an array of 15 rows and 15 columns. Each cell contains two identical holes, one at the center and one in a randomly chosen corner. The size of the disks varies logarithmically from 0.3 to 8 mm in both diameter and depth. For each exposure, four images were acquired and the CDRAD phantom was randomly repositioned after each exposure. The repositioning allows one to get images with different phantom-object positions with respect to the pixels of the detector. In this way, we avoided that a small detail always remained in the same detector region. Images were acquired at the same exposures used for the physical characterization.

Reading CD phantoms by human observers is a very tedious and time consuming task. To overcome this shortcoming, automatic methods have been developed and evaluated.[18,19] Such methods reduce *inter*- and *intra*observer subjective variability and dramatically decrease the time needed to analyze scores of images. Our group has developed a software that automatically reads the CDRAD images,[13] which is written in IDL™ (RSI, Pearl East Circle Boulder, CO) and can be freely downloaded at www.df.unibo.it/medphys. First of all, the software requires a manual registration of the phantom. After that, it scans all the cells of the phantom. For each cell a few parameters for the central disk are estimated for obtaining the CD curve. Specifically, a few ROIs positioned within the central details and on the background of the cell are used to calculate the signal-to-noise ratio (SNR) for each cell of the phantom. The noise is computed as the standard deviation of the gray-level distribution of the background. Finally, the contrast detail curve is determined by calculating the inverse of the SNR as a function of the contrast. For each exposure, a contrast detail curve was obtained by averaging results of the four images acquired with that exposure. More details about the procedure used to estimating the automatic CD curves can be found in Ref. 13. We completed the statistical analysis of the CD curves by using the SPSS package (version 13.0; SPSS, Inc., Chicago, IL). We tested the statistically significantly difference of two CD curves by performing a nonparametric test (Mann–Whitney). We tested both the curves consisting of all the phantom details together and also the subset of data including only details with a diameter greater than 1 mm. A $p$ value of less than 0.05 was considered to indicate a statistically significant difference between two curves.

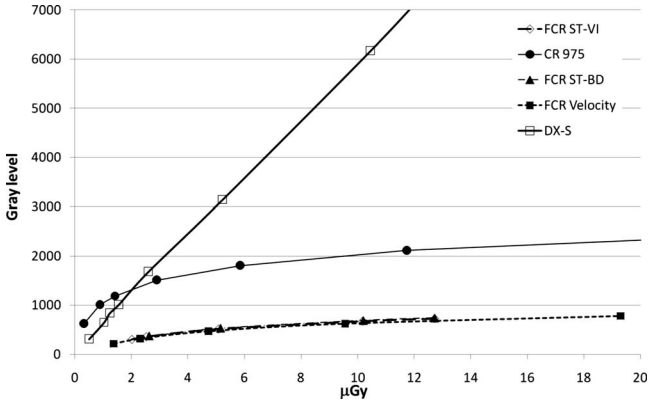


FIG. 1. Response curves for the five analyzed CR systems. The Agfa unit has a linear response, whereas all other systems present a logarithmic response. Fitting curves used for linearizing the CR responses are shown in Table II.

TABLE II. Functions used for fitting the response curves shown in Fig. 1 with the corresponding $R^2$ value for quantifying the goodness of the fit. For all the functions, $y$ stands for the gray-level value of the images, whereas $x$ stands for exposure (measured in $\mu$Gy). All systems present a logarithm response, except the Agfa unit, which shows a linear behavior over the entire range of the investigated exposures.

| CR system | Fitting function | $R^2$ value |
|---|---|---|
| FCR ST-VI | $y=229\log(x)+142.8$ | 0.9999 |
| FCR ST-BD | $y=233\log(x)+146.5$ | 0.9999 |
| CR975 | $y=421\log(x)+1069$ | 0.9989 |
| FCR Velocity | $y=214\log(x)+141.4$ | 0.9995 |
| DX-S | $y=588x+76.1$ | 0.9998 |

## III. RESULTS

### III.A. Physical characterization

The response curves of the five systems are reported in Fig. 1. The fitting curves used to linearize CR response and the corresponding goodness of fit ($R^2$) are shown in Table II. All systems presented a logarithm response, except the Agfa unit, which showed a linear behavior over the entire range of investigated exposure levels. All the systems manufactured by FUJIFILM basically present the same curve, whereas the CR975 has still a logarithmic response, but it can provide a wider dynamic range, thanks to the 12 bit quantization. We considered the fitting functions shown in Table II for linearizing all the images used for the physical characterization.

Presampling MTF curves resulting from the average of the horizontal and vertical directions for the five CR systems are shown in Fig. 2. No appreciable variations in MTF were found when changing the exposure value. In Fig. 3 the differences between the MTFs calculated along the two main directions are plotted.

Figure 4 shows an example of the 2D NNPS for an exposure of 5 $\mu$Gy. Figure 5 shows the 1D NNPS results obtained on the radial direction at 45° from the 2D NNPS, ignoring values along the principal axes.

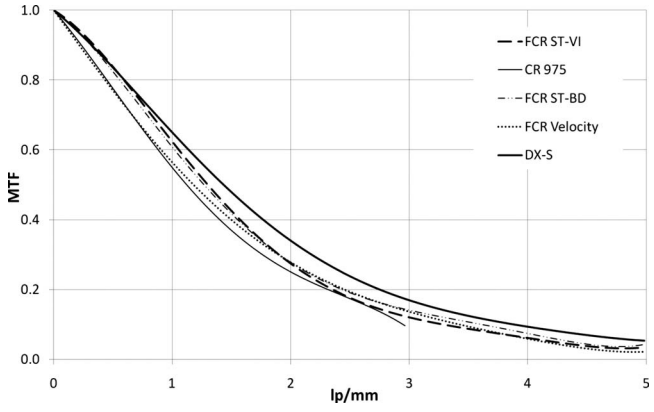


FIG. 2. Presampling MTF curves for the five CR systems. The plot shows the MTF as resulting from the average of the two directions (horizontal and vertical). It is worth noting that the DX-S unit presents a slightly better spatial resolution even if it exploits a thicker scintillator, thanks to the columnar structure of the phosphor.

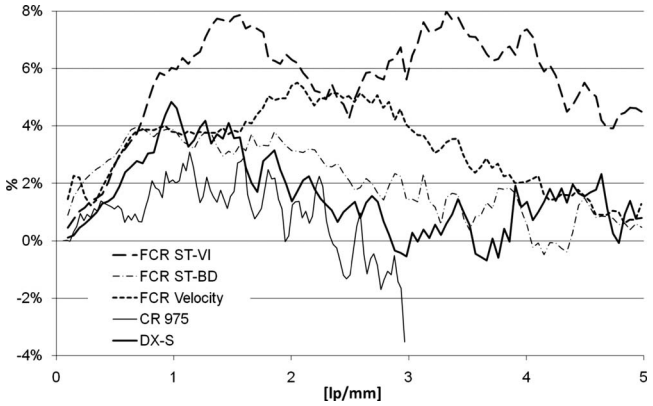


FIG. 3. Plot showing the difference in the MTF calculated on the two directions for the five CR systems. Some systems show very small differences (especially the Kodak and the Agfa units), whereas others present more clear variations in the MTF in the two directions (especially FCR ST-VI and FCR velocity).

Figure 6 shows the RSD plotted as a function of the air kerma for the five systems. The experimental data were fitted with the function given in Eq. (1) and the fitting functions coefficients are summarized in Table III. These parameters can help understand the different components of the noise.

Figure 7 shows the product of NNPS multiplied by the exposure (air kerma) as a function of the spatial frequency. This product remains constant for every exposure when a detector is quantum noise limited.

Finally, DQE results are shown in Fig. 8 for the three investigated exposure values.

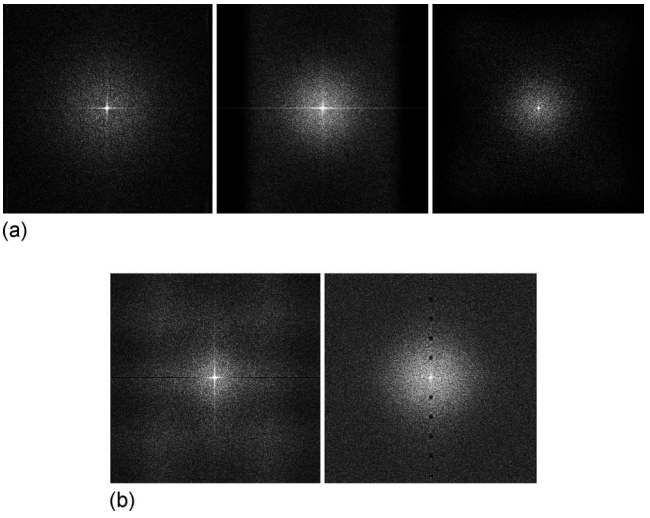


FIG. 4. Example of 2D NNPS image for the five systems. Top row: CR975 (left), FCR ST-VI (center), and FCR ST-BD (right). Bottom row, FCR Velocity (left), DX-S (right). All systems, except CR975, seem to present a software filtering acting differently on the two directions. This effect can be observed undoubtedly for the FCR ST-VI unit: It shows a clear difference between the NNPS on the two directions. A slighter but marked difference is present also for FCR Velocity. The different behaviors for the two directions should be due to the fact that FUJIFILM systems use an antialiasing filter. The DX-S unit presents some frequencies missing along one axis, probably caused by a sort of notch filter applied to the images. The window/level of the pictures has been modified for getting a better visualization.

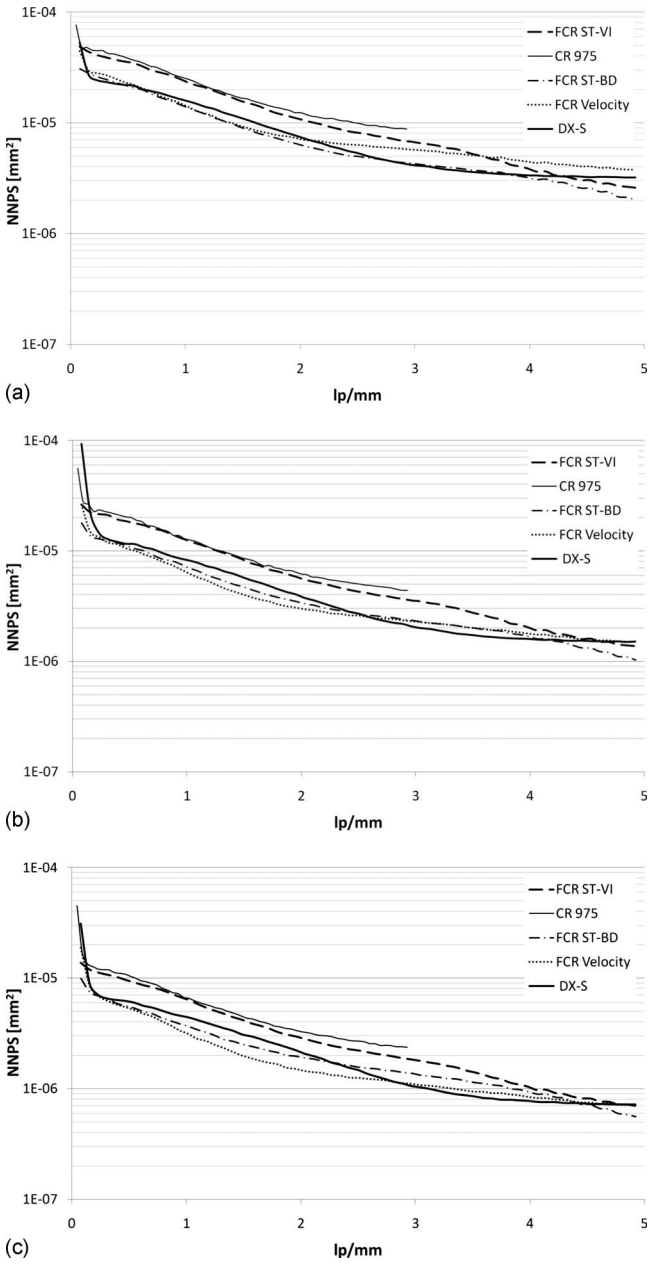


FIG. 5. 1D NNPS for the five systems at the three investigated exposures: (a) 2.5 $\mu$Gy, (b) 5 $\mu$Gy, and (c) 10 $\mu$Gy. 1D NNPS is obtained on the radial direction from the 2D NNPS.

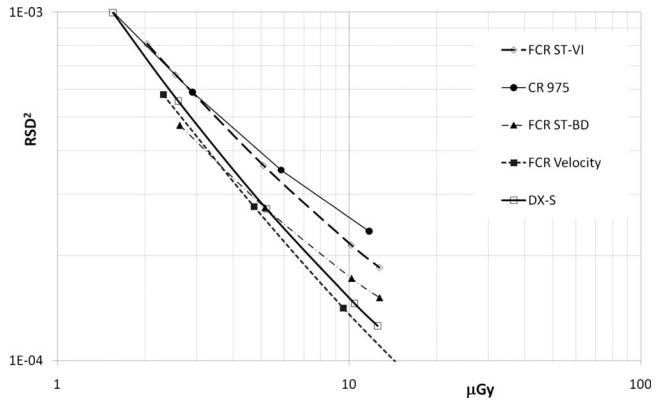


FIG. 6. RSD analysis: Experimental data for $RSD^2$ values (points on the graph) and the fitting curves used for estimating the various components of the system's noise, as described in Eq. (1). The coefficients of the fitting functions are summarized in Table II.

### III.B. Contrast detail analysis

Figure 9 shows the CD curves obtained by the five systems at an exposure of 10 $\mu$Gy. The systems based on the latest technologies offer better results, with respect to the conventional CR units, especially for medium-large details. The same trend for the CD curves can be observed at the other two investigated exposures even if for the lowest exposure no statistically significant differences were observed.

## IV. DISCUSSION

The two systems based on CCD detectors (FCR Velocity and DX-S) have a different response curve. In fact, the DX-S unit preserves the linear response typical of CCD detectors, whereas for the FCR Velocity system, a logarithmic transform is applied during the reading step.

The best MTF is obtained with the DX-S unit. In fact, even if the phosphor layer used for this system is thicker than in most of the other systems, there is no appreciable deterioration of the MTF, thanks to its columnar structure. This suggests that it is possible to improve efficiency and noise properties, without reducing too much the spatial resolution. On the other hand, the even thicker phosphor used for FCR Velocity does not allow for MTF values comparable to those from the DX-S. Most likely, the thickness of the phosphor for FCR Velocity unit was chosen to give spatial resolutions comparable to those of the standard CR systems. The unit based on dual-side reading presents basically the same MTF of the FCR ST-VI system in spite of the thicker phosphor employed. Although all systems use a mechanical scanning along one direction, we note that some of them (i.e., Kodak and Agfa units) presented small differences, whereas others (especially FCR ST-VI and FCR Velocity) showed more accentuated variations. These results could be also explained by taking into account the 2D NNPS shown in Fig. 4. All systems except CR975 appear to use a software filtering acting differently on the two directions. In particular, the FCR ST-VI unit has a remarkable difference between the NNPS on the two directions as if a low pass filter was used only on the horizontal direction. This effect was detectable with lesser intensity in the FCR Velocity system most likely because of the different reading technologies (line scan), while it was practically undetectable in the dual-side reading technology (FCR ST-DB). In this case, the different behaviors along the two directions appear to be due to an antialiasing filter used in the majority of FUJIFILM systems, as noted in other studies.[11,20,21] The FCR Velocity spectrum shows very low values along the horizontal axis: We believe that this contribution is lowered through a software filtering process. The Kodak and Agfa systems have an almost perfectly isotropic response, as shown also by the small differences in their MTF along the two directions. The DX-S unit has a

TABLE III. Values of the main noise components for the five systems, as estimated by the RSD analysis.

| Components | FCR ST-VI | FCR ST-BD | CR975 | FCR Velocity | DX-S |
|---|---|---|---|---|---|
| Poisson: $\alpha$ | $1.5\times10^{-3}$ | $1.1\times10^{-3}$ | $1.4\times10^{-3}$ | $1.2\times10^{-3}$ | $1.2\times10^{-3}$ |
| Multiplicative: $\beta$ | $6.6\times10^{-5}$ | $6.8\times10^{-5}$ | $1.2\times10^{-4}$ | $1.7\times10^{-5}$ | $3.0\times10^{-5}$ |
| Additive: $\gamma$ | $1.0\times10^{-10}$ | $8.9\times10^{-6}$ | $1.0\times10^{-8}$ | $3.2\times10^{-4}$ | $5.2\times10^{-4}$ |

spectrum with some equispaced hollows along the vertical axis, as already noted by Mackenzie *et al.*[22] They attributed their presence to the image processing that compensates for the variation in transmission from the linear lens array. We agree that these troughs are caused by image processing (or filtering) whose effect is the same as that obtained with a notch filter applied during the reading process.[23]

It is worth noting as the two systems based on the dated technology (FCR ST-VI and CR975) have a remarkably higher noise for all the investigated exposures. This differ-

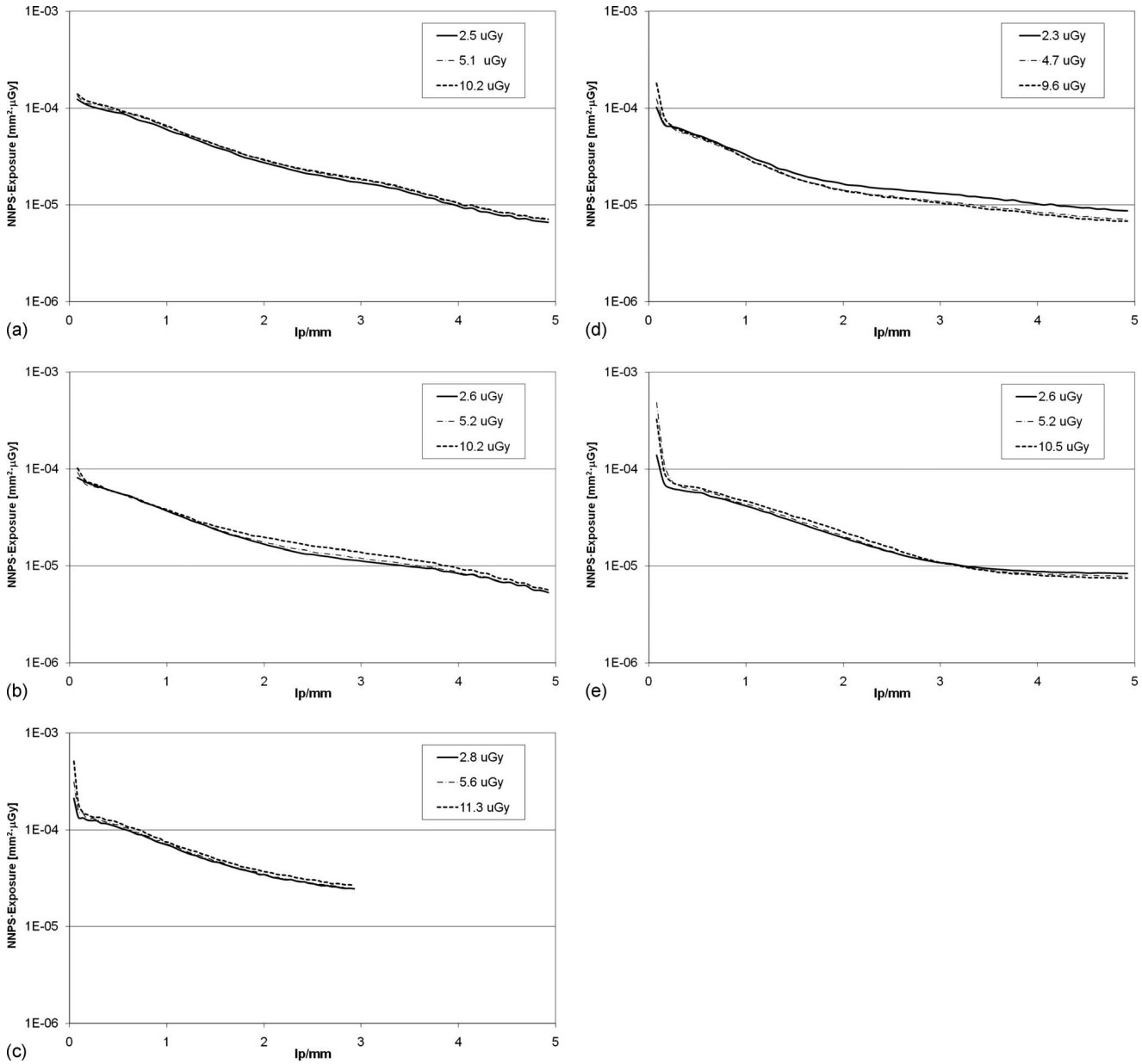


FIG. 7. NNPS multiplied by air kerma for the five systems and three different exposures (2.5, 5, and 10 $\mu$Gy). The five plots represent the investigated systems: (a) FCR ST-VI, (b) FCR ST-BD, (c) CR975, (d) FCR Velocity, and (e) DX-S. This product should be independent from the exposure, for a strictly quantum noise limited detector.

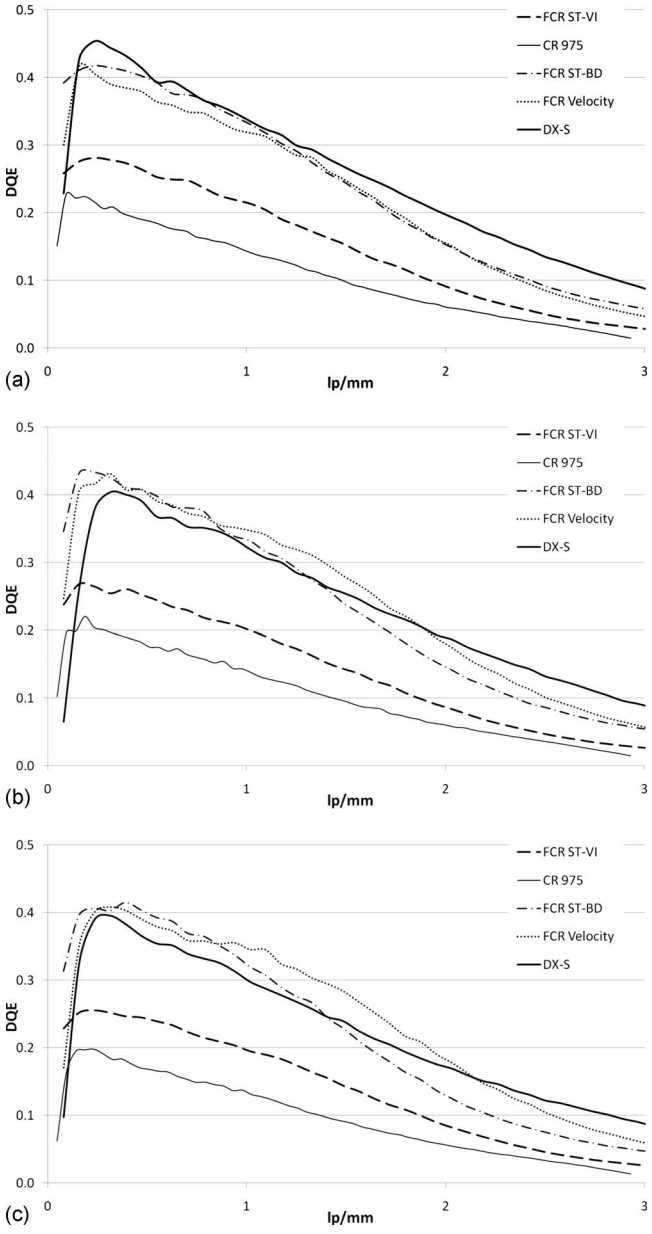


FIG. 8. DQE for the five systems at the three investigated exposures: (a) 2.5 $\mu$Gy, (b) 5 $\mu$Gy, and (c) 10 $\mu$Gy. The two systems based on the more outdated technology (granular phosphor with single-side reading) present DQE values worse than the other systems in the entire range of frequencies for all the investigated exposures. All the detectors show DQE nearly independent of the exposure, revealing a quantum noise limited condition.

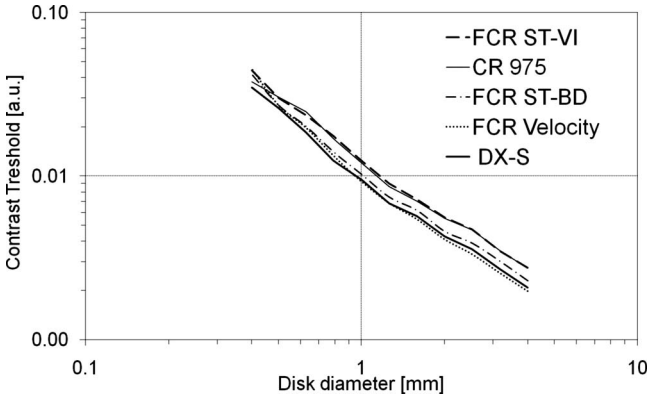


FIG. 9. Contrast detail curves for the five CR systems at an exposure of 10 $\mu$Gy. The trend of the CD curves for the other exposures is similar to this one. The three CR systems based on the latest technologies show a better response also in terms of CD visibility.

ence is evident at frequencies up to about 3.5 lp/mm, while it diminishes at higher frequencies. Again, we note that this is connected to the improved detection efficiency of the three advanced systems as a result of the greater thickness of the phosphor layer (for FCR Velocity and DX-S) and the dual-side reading (for FCR ST-BD).

A major outcome of the RSD analysis is that for all the systems, the statistical noise is dominant: In fact, the multiplicative and additive components are always smaller and often negligible with respect to the statistical noise. As a consequence, this suggests that all the CR systems examined in this study are able to work in quantum noise limited condition. We also note that the two units based on the latest technology present an higher additive noise and a smaller multiplicative noise with respect to the other systems. The high additive noise should be related to the CCDs used in line-scanning technology, whose additive noise is intrinsically higher than that of the PMTs used in the standard CR systems.[1,12]

By looking at the product of NNPS and exposure, we notice that all the systems, thanks to their low additive noise, are limited by statistical noise for the entire range of investigated exposures. Further, at the highest exposure (10 $\mu$Gy) a slightly worse response is observed in detectors with higher multiplicative noise (FCR ST-VI, FCR ST-BD, and CR975) due to the overwhelming multiplicative component.

Systems based on the new technologies show DQE values roughly twice as better than those for standard CR units—especially at low frequencies—as a consequence of the overall improved efficiency due to increased thickness of the columnar phosphor (FRC Velocity and DX-S), and to the dual-side reading (FCR ST-BD). As for the line-scanning technology, at low exposures, the DX-S showed a slightly better performance compared to FCR Velocity, while results are inverted for high exposures, especially at middle-low frequencies. This could be related to the thicker phosphor used in FRC Velocity and to the fact that the higher multiplicative noise of DX-S increases its weight at high exposures. Dual-side reading and line-scanning systems are quite similar, but the latter technology shows an improvement at frequencies higher than 1.5 lp/mm. It is worth remarking that at low frequencies the units based on columnar phosphors have DQE values quite similar to those of the dual-side reading, whereas differences appear at high frequencies, especially for the DX-S unit. This improvement is due to the better response in terms of the spatial resolution of the needle-shaped scintillator. All the systems have DQE almost independent of the exposure, revealing a quantum noise limited condition for all the investigated exposures. These results agree reasonably with other results obtained for the same systems in similar conditions.[5,12,21,24] The improved DQE

can be exploited either to enhance the image quality, or to reduce the dose to the patients, as already assessed by other researchers.[25] The DQE of the three best systems investigated in this paper is also comparable to some of the flat-panel detectors for radiography available in the market.[26–28]

The CD results confirm that the improved efficiency helps achieve a lower contrast threshold. In fact, for details with a diameter greater than 1 mm, the FCR ST-VI and the CR975 systems present a statistically significant different response, with respect of both the FCR Velocity unit (with $p<0.01$) and the DX-S system ($p<0.05$). Our results agree with other studies that showed that CR systems with needle phosphors have superior image quality when compared to the conventional ones.[29,30]

## V. CONCLUSION

In this paper, we compared five different CR systems for radiology based on three different technologies: Conventional powder phosphors with single-side reading, powder phosphors with dual-side reading, and columnar phosphors with line scanning. The most advanced units based on columnar phosphors provide spatial resolutions not lower to those obtained with conventional CR systems in spite of their thicker phosphors. On the other hand, the greater thickness of the columnar phosphor allows for an improved efficiency and hence better noise properties. In fact, the standard CR systems present a remarkable higher NNPS at all investigated exposures, especially at frequencies up to 3.5 lp/mm. As a consequence, the three units based on columnar phosphors and line-scanning reading, or granular phosphor and dual-side reading, provide DQE values noticeably better than the conventional CR systems. Actually, DQE of about 40% are easily achievable at all the investigated exposures. These values are comparable to those obtained with some of the flat-panel detectors for radiography available on the market. The contrast detail analysis by means of an automatic reading of the CDRAD phantom basically confirms the superiority of the most advanced systems.

In conclusion, this study suggests that CR systems based on the most advanced technologies (dual-side or line-scanning reading and columnar phosphors) provide a remarkable improvement in performance with respect to conventional CR units, giving results comparable to those achieved by most flat-panel detectors for radiography.

[a]Author to whom correspondence should be addressed. Electronic mail: nico.lanconelli@unibo.it; URL: www.bo.infn.it/~lanconelli; Present address: Dipartimento di Fisica, Viale Berti-Pichat 6/2, I-40127 Bologna, Italy; Telephone: +39-051-2095136; Fax: +39-051-2095047.

[1]J. A. Rowlands, "The physics of computed radiography," Phys. Med. Biol. **47**, R123–R166 (2002).
[2]A. R. Cowen, A. G. Davies, and S. M. Kengyelics, "Advances in computed radiography systems and their physical imaging characteristics," Clin. Radiol. **62**, 1132–1141 (2007).
[3]H. P. McAdams, E. Samei, J. Dobbins III, G. D. Tourassi, and C. E. Ravin, "Recent advances in chest radiography," Radiology **241**, 663–683 (2006).
[4]C. Schaefer-Prokop, U. Neitzel, H. W. Venema, M. Uffmann, and M. Prokop, "Digital chest radiography: An update on modern technology, dose containment and control of image quality," Eur. Radiol. **18**, 1818–1830 (2008).
[5]K. A. Fetterly and B. A. Schueler, "Performance evaluation of a computed radiography imaging device using a typical 'front side' and novel 'dual side' readout storage phosphors," Med. Phys. **33**, 290–296 (2006).
[6]S. Arakawa, H. Yasuda, K. Kohda, and T. Suzuki, "Improvement of image quality in CR mammography by detection of emissions from dual sides of an imaging plate," Proc. SPIE **3977**, 590–600 (2000).
[7]R. Schaetzing, R. Fasbender, and P. Kersten, "New high-speed scanning technique for computed radiography," Proc. SPIE **4682**, 511–520 (2002).
[8]P. Leblans, L. Struye, and P. Willems, "New needle-crystalline CR detector," Proc. SPIE **4320**, 59–67 (2001).
[9]J. Frankenberger, S. Mair, C. Herrmann, J. Lamotte, and R. Fasbender, "Reflective and transmissive CR scanhead technology on needle image plates," Proc. SPIE **5745**, 499–510 (2005).
[10]H. Nanto, Y. Takei, A. Nishimura, Y. Nakano, T. Shouji, T. Yanagita, and S. Kasai, "Novel x-ray image sensor using CsBr:Eu phosphor for computed radiography," Proc. SPIE **6142**, 2W–1-9 (2006).
[11]L. Riccardi, M. C. Cauzzo, R. Fabbris, E. Tonini, and R. Righetto, "Comparison between a built-in 'dual side' chest imaging device and a standard 'single side' CR," Med. Phys. **34**, 119–126 (2007).
[12]A. Mackenzie and I. D. Honey, "Characterization of noise sources for two generations of computed radiography systems using powder and crystalline photostimulable phosphors," Med. Phys. **34**, 3345–3357 (2007).
[13]A. Nitrosi, M. Bertolini, G. Borasi, A. Botti, A. Barani, S. Rivetti, and L. Pierotti, "Application of QC_DR software for acceptance testing and routine quality control of direct digital radiography systems: Initial experiences using the Italian Association of Physicist in Medicine Quality Control Protocol," J. Digit Imaging **22**, 656–666 (2009).
[14]International Electrotechnical Commission, "Medical diagnostic x-ray equipment—Radiation conditions for use in the determination of characteristics," IEC-61267, Geneva, Switzerland, 2003.
[15]E. Samei, M. J. Flynn, and D. A. Reimann, "A method for measuring the presampled MTF of digital radiographic systems using an edge test device," Med. Phys. **25**, 102–113 (1998).
[16]U. Neitzel, S. Günther-Kohfahl, G. Borasi, and E. Samei, "Determination of the detective quantum efficiency of a digital x-ray detector: Comparison of three evaluations using a common image data set," Med. Phys. **31**, 2205–2211 (2004).
[17]S. Rivetti, N. Lanconelli, R. Campanini, M. Bertolini, G. Borasi, A. Nitrosi, C. Danielli, L. Angelini, and S. Maggi, "Comparison of different commercial FFDM units by means of physical characterization and contrast-detail analysis," Med. Phys. **33**, 4198–4209 (2006).
[18]A. Pascoal, C. P. Lawinski, I. Honey, and P. Blake, "Evaluation of a software package for automated quality assessment of contrast detail images—Comparison with subjective visual assessment," Phys. Med. Biol. **50**, 5743–5757 (2005).
[19]K. C. Young, J. H. Cook, J. M. Oduko, and H. Bosmans, "Comparison of software and human observers in reading images of the CDMAM test object to assess digital mammography systems," Proc. SPIE **6142**, 614206.1–614206.13 (2006).
[20]E. Samei and M. J. Flynn, "An experimental comparison of detector performance for computer radiography systems," Med. Phys. **29**, 447–459 (2002).
[21]P. Monnin, Z. Holzer, R. Wolf, U. Neitzel, P. Vock, F. Gudinchet, and F. R. Verdun, "An image quality comparison of standard and dual-side read CR systems for pediatric radiology," Med. Phys. **33**, 411–420 (2006).
[22]A. Mackenzie, I. D. Honey, D. P. Emerton, P. Blake, H. Cole, and C. P. Lawinski, "Computed radiography (CR) systems for general radiography. Agfa Healthcare DX-S," Report No. 06004, Centre for Evidence-Based Purchasing, London, 2006.
[23]I. N. Bankman, *Handbook of Medical Imaging: Processing and Analysis*, 1st ed. (Academic, San Diego, 2000).
[24]K. Shimada, H. Yasuda, S. Arakawa, T. Kuwabara, A. Takasu, Y. Iwabuchi, and M. Katou, "Comparison in image quality and noise component of columnar phosphor plate and powder phosphor plate," Proc. SPIE **6510**, 651044.1–651044.8 (2007).
[25]S. Wirth, M. Treitl, M. F. Reiser, and M. Körner, "Imaging performance with different doses in skeletal radiography: Comparison of a needle-structured and a conventional storage phosphor system with a flat-panel detector," Radiology **250**, 152–160 (2009).
[26]G. Borasi, A. Nitrosi, P. Ferrari, and D. Tassoni, "On site evaluation of three flat panel detectors for digital radiography," Med. Phys. **30**, 1719–1731 (2003).

[27]P. Monnin, D. Gutierrez, S. Bulling, D. Lepori, J. F. Valley, and F. R. Verdun, "Performance comparison of an active matrix flat panel imager, computed radiography system, and a screen-film system at four standard radiation qualities," Med. Phys. **32**, 343–350 (2005).
[28]G. Borasi, E. Samei, M. Bertolini, A. Nitrosi, and D. Tassoni, "Contrast-detail analysis of three flat panel detectors for digital radiography," Med. Phys. **33**, 1707–1719 (2006).
[29]J. M. Fernandez, J. M. Ordiales, E. Guibelalde, C. Prieto, and E. Vano, "Physical image quality comparison of four types of digital detector for chest radiology," Radiat. Prot. Dosim. **129**, 140–143 (2008).
[30]M. Körner, M. Treitl, R. Schaetzing, K. J. Pfeifer, M. Reiser, and S. Wirth, "Depiction of low-contrast detail in digital radiography: Comparison of powder- and needle-structured storage phosphor systems," Invest. Radiol. **41**, 593–599 (2006).